Lasers in Manufacturing Conference 2015

Laser processing of lithium iron phosphate battery electrodes

Adrian H.A. Lutey[a]*, Alessandro Fortunato[a], Maurizio Fiorini[b], Simone Carmignato[c], Alessandro Ascari[a]

[a]*DIN, Università di Bologna, viale Risorgimento 2, Bologna 40136, Italy*
[b]*DICAM, Università di Bologna, via Terracini 28, Bologna 40131 Italy*
[c]*DTG, Università degli Studi di Padova, Stradella San Nicola 3, Vicenza 36100 Italy*

Abstract

Lithium iron phosphate (LFP) battery electrodes are exposed to laser radiation at 100 mm/s and 1000 mm/s while systematically varying pulse duration (4-200 ns), repetition rate (20-1000 kHz) and average power (1-150 W). An optical profiler operating in confocal mode is utilised to establish material removal efficiency in all cases, while scanning electron and Raman microscopes are employed to determine macroscopic, microstructural and chemical changes near the cut edges. The laser pulse fluence ranges leading to lowest minimum cutting power at 100 mm/s are found to be 35–40 J/cm^2 (100 kHz) and 100–110 J/cm^2 (20 kHz) for the cathode and anode, respectively. The same laser parameters are found to result in the smallest clearance width of the upper coating layer and the smallest defects. By increasing the exposure velocity to 1 m/s and scaling the average laser power and repetition rate proportionally, clearance width and defect size are found to reduce moderately, while chemical and microstructural degradation of the active layers is all but eliminated. This study confirms the process as a viable alternative to mechanical blanking.

Keywords: Laser Ablation; Lithium Ion; $LiFePO_4$; Graphite

1. Introduction

Rapidly growing interest in hybrid-electric vehicles (HEVs) and electric vehicles (EVs) has led to intensive research into high density electrical energy storage, as exhibited by Peterson and Whitacre, 2011. At present, capacity, recharge time and cost remain the principle limiting factors to the fast uptake of HEVs and EVs (Scrosati and Garche, 2010). A number of authors, including Pollet et al., 2012, have highlighted the potential of the lithium iron phosphate (LFP) battery in this application due to its high energy density, long cycle life, inherent thermal stability and composition that is both inexpensive and non-toxic. Despite these advantages, production costs remain high due to the use of mechanical blanking devices for electrode sizing that require regular servicing and replacement. Lutey et al., 2015, have shown that use of laser technology

* Corresponding author. Tel.: +39 051 2093416
E-mail address: adrian.lutey2@unibo.it

for cutting operations offers potential for lowering ongoing costs. The present work sees 1064 nm nanosecond pulsed laser exposures performed on LFP battery electrodes at 100 mm/s and 1000 mm/s while varying the pulse duration, repetition rate and average laser power. Incisions and cuts are analysed with an optical profiler operating in confocal mode to determine material removal efficiency. A scanning electron microscope (SEM) is utilised to observe macroscopic defects along the cut edge and a Raman microscope is employed to resolve potential chemical and microstructural changes arising from laser exposure.

2. Experimental Setup

Commercial LFP battery electrodes were utilised for the experiments. The cathode consisted of 20 µm aluminium coated on both sides with 45 µm $LiFePO_4$, the anode of 10 µm copper coated on both sides with 47 µm polycrystalline graphite. Laser exposures were performed with two laser sources over seven discrete parameter groups (Tab. 1), allowing comparison of the effects of process parameters on the resulting incision or cut. The best results obtained for the cathode at 100 mm/s (parameter group 3) were extrapolated to 1000 mm/s to form group 7. The electrodes were held horizontally by a custom built vacuum mounting with cutouts to avoid contact between the electrode and mounting for at least 3 mm to either side of the exposed area. Where complete cuts did not result for parameter groups 1-6, the incision was analysed in ten sections with a 3D optical profiler operating in confocal mode (Balcon et al., 2012). Where the electrode films were completely cut during laser exposure, images of the resulting cut edges were obtained via SEM analysis. A Raman microscope with 532 nm He-Ne laser was then utilised to acquire Raman line map spectra across the HAZ of selected samples. In line with previous studies conducted by Markevich et al., 2011, a Raman laser power of 1 mW was utilised with a 1.2-2.4 µm spot size to avoid oxidative decomposition of the electrode materials during measurement. Acquisitions were performed for a maximum duration of 90 s or until a signal-to-noise ratio of 500 was attained for the most intense peak.

Table 1: Process parameters utilised for the experiments. [a]Measured values at sample surface.

Parameter group	1	2	3	4	5	6	7
Pulse duration (ns)	4	30	30	200	200	200	65
Repetition rate (kHz)	500	500	100	500	100	20	1000
Spot diameter (µm)	25	25	25	25	25	25	42
Max. average power[a] (W)	19	19.2	18.8	19.1	18.8	18.7	150
Max. pulse energy[a] (µJ)	38	38	188	38	188	935	150
Max. fluence[a] (J/cm²)	15	15	74	15	74	369	22
Exposure velocity (mm/s)	100	100	100	100	100	100	1000

3. Results and discussion

3.1. Incision depths

In almost all cases, complete removal of the upper coating layer took place for the lowest tested average laser power, 4 W, while complete film penetration required up to 17 W. The incision depth was a piece-wise function of average laser power, with no partial incision of the underside coating layer prior to complete film penetration. These results indicated that the process was dominated by the metallic conductor layers, despite their low thicknesses. For constant repetition rate, minimum cutting power was lowest for shorter

laser pulses; however, cutting efficiency exhibited greater dependence on the repetition rate with 100 kHz and 20 kHz leading to the lowest minimum cutting power for the cathode and anode, respectively. Lowest minimum cutting power was required with 30 ns pulses of fluence 35-40 J/cm^2 (group 3 at 9 W) for the cathode and 200 ns pulses of fluence 100-110 J/cm^2 (group 6 at 5.5 W) for the anode.

3.2. SEM analysis

At 100 mm/s, the same laser parameters leading to highest cutting efficiency were found to result in the smallest clearance width of the upper coating layer and the smallest defects: 20 µm and 5 µm, respectively, for the cathode and 30 µm and <1 µm for the anode. Noting that highest cutting efficiency and quality was achieved for the cathode at 100 mm/s with parameter group 3, extrapolation to 1000 mm/s yielded parameter group 7. SEM images for complete cuts achieved at 1000 mm/s with this parameter group are presented in Fig. 1. Removal of the active layers is restricted to regions directly exposed to the incident laser beam, with clearance widths of approximately 25 µm and small spherical defects on the cathode, <5 µm in size.

3.3. Raman analysis

Raman analysis of cuts acheived at 100 mm/s revealed the presence of α-Fe_2O_3 oxidation products in the visible heat affected zone (HAZ) of the cathode and degradation of the polycrystalline graphite structure to a less ordered carbon structure in the anode. Figure. 2 shows the Raman line map spectra for electrode cuts achieved with parameter group 7 at 1000 mm/s. Measurement locations are indicated on the adjacent microscope images. The active phase of the cathode, olivine LFP, is indicated by a peak at 951 cm^{-1}, while peaks at 1336 cm^{-1} and 1602 cm^{-1} correspond to carbon black added to improve the electronic conductivity of the active phase. The spectrum of the anode is characterised by bands at 1585 cm^{-1} and 1351 cm^{-1}, corresponding to G (crystalline) and D (disordered) graphite structures. The D/G ratio of the unexposed anode material is 0.5, corresponding to polycrystalline graphite. Though the cathode exhibits some discolouration due to degradation of the binder material, the Raman spectrum remains unchanged at all points approaching the cut edge. The anode exhibits some degradation of the crystalline graphite structure at approximately 50 µm from the cut edge, immediately outside the clearance zone, exhibited by an increase in the D/G ratio. Chemical and microstructural changes were vastly reduced at high exposure velocity. The result is a good quality cut at speeds that can effectively compete with mechanical blanking devices.

4. Conclusion

Laser cutting of LFP battery electrodes offers potential for cost savings in high volume production facilities by eliminating the need for mechanical blanking devices that require regular servicing and replacement. By extrapolating the optimum repetition rate and average laser power for the cathode at 100 mm/s to 1000 mm/s, high quality cuts were achieved on both electrodes at speeds that could effectively compete with mechanical blanking. Though the characteristics of the cut edge are different for laser cutting, with active coating layer clearance and the presence of <5 µm spherical defects on the cathode, the method shows promise as a viable alternative to mechanical blanking.

Acknowledgements

The authors would like to thank IPG Italia S.R.L. for allowing and assisting with the utilisation of their laser source for completion of this work.

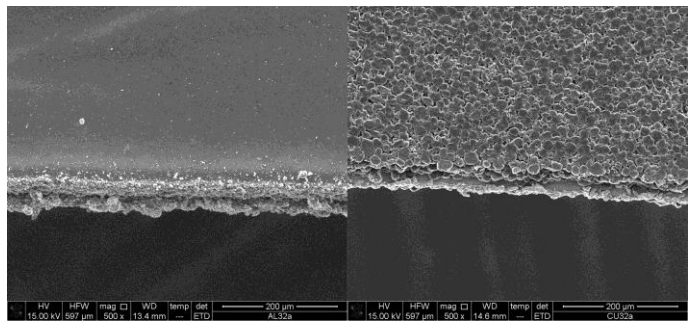

Fig. 1.SEM images of cut edges with parameter group 7 for cathode (left) and anode (right).

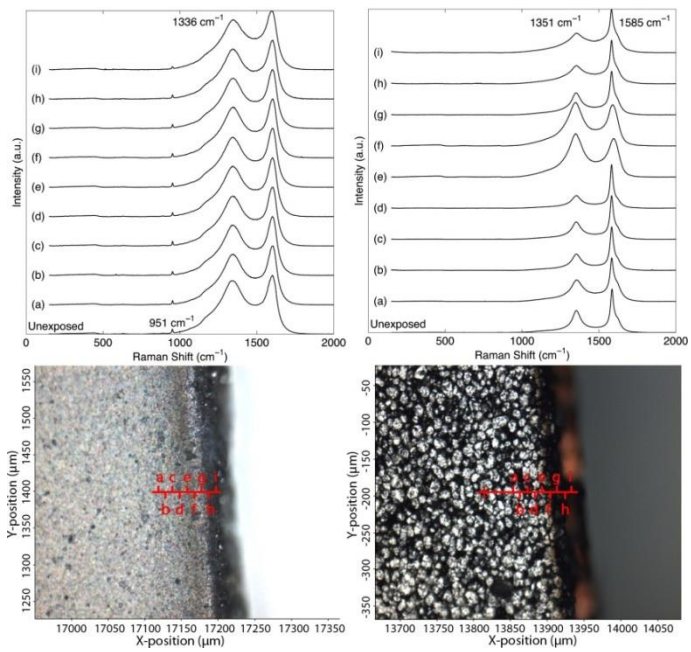

Fig. 2. Raman spectra and microscope images for cathode (left) and anode (right) with parameter group 7.

References

Balcon, M., Carmignato, S., Savio, E., 2012. Performance verification of a confocal microscope for 3D metrology tasks, Quality – Access to Success 13, pp. 63–66.

Lutey, A., Fortunato, A., Ascari, A., Carmignato, S., Leone C., 2015. Laser cutting of lithium iron phosphate battery electrodes: characterization of process efficiency and quality, Optics & Laser Technology 65, pp. 164–174.

Markevich, E., Sharabi, R., Haik, O., Borgel, V., Salitra, G., Aurbach, D., Semrau, G., Schmidt, M., Schall, N., Stinner, C., 2011. Raman spectroscopy of carbon-coated LiCoPO4 and LiFePO4 olivines, Journal of Power Sources 196, pp. 6433-6439.

Peterson, S., Whitacre, J., Apt, J., 2011. Net air emissions from electric vehicles: the effect of carbon price and charging strategies, Environmental Science & Technology 45, pp. 1792–1797.

Pollet, B., Staffell, I., Shang, J., 2012. Current status of hybrid, battery and fuel cell electric vehicles: from electrochemistry to market prospects, Electrochimica Acta 84, pp. 235–249.

Scrosati, B., Garche, J., 2010. Lithium batteries: status, prospects and future, Journal of Power Sources 195, pp. 2419–2430.